Patient-specific radiation dose and cancer risk estimation in CT: Part II. Application to patients

Xiang Li
Medical Physics Graduate Program, Carl E. Ravin Advanced Imaging Laboratories, Department of Radiology, Duke University Medical Center, Durham, North Carolina 27705

Ehsan Samei[a)]
Carl E. Ravin Advanced Imaging Laboratories, Department of Radiology, Medical Physics Graduate Program, Department of Physics, and Department of Biomedical Engineering, Duke University Medical Center, Durham, North Carolina 27705

W. Paul Segars
Carl E. Ravin Advanced Imaging Laboratories, Department of Radiology, Medical Physics Graduate Program, Duke University Medical Center, Durham, North Carolina 27705

Gregory M. Sturgeon
Carl E. Ravin Advanced Imaging Laboratories, Department of Radiology, Duke University Medical Center, Durham, North Carolina 27705 and Department of Biomedical Engineering, University of North Carolina, Chapel Hill, North Carolina 27599

James G. Colsher
Department of Radiology, Duke University Medical Center, Durham, North Carolina 27705

Greta Toncheva
Duke Radiation Dosimetry Laboratory, Department of Radiology, Duke University Medical Center, Durham, North Carolina 27705

Terry T. Yoshizumi
Duke Radiation Dosimetry Laboratory, Department of Radiology, Medical Physics Graduate Program, Duke University Medical Center, Durham, North Carolina 27705

Donald P. Frush
Division of Pediatric Radiology, Department of Radiology, Medical Physics Graduate Program, Duke University Medical Center, Durham, North Carolina 27710

(Received 18 June 2010; revised 17 September 2010; accepted for publication 21 October 2010; published 22 December 2010)

Purpose: Current methods for estimating and reporting radiation dose from CT examinations are largely patient-generic; the body size and hence dose variation from patient to patient is not reflected. Furthermore, the current protocol designs rely on dose as a surrogate for the risk of cancer incidence, neglecting the strong dependence of risk on age and gender. The purpose of this study was to develop a method for estimating patient-specific radiation dose and cancer risk from CT examinations.

Methods: The study included two patients (a 5-week-old female patient and a 12-year-old male patient), who underwent 64-slice CT examinations (LightSpeed VCT, GE Healthcare) of the chest, abdomen, and pelvis at our institution in 2006. For each patient, a nonuniform rational B-spine (NURBS) based full-body computer model was created based on the patient's clinical CT data. Large organs and structures inside the image volume were individually segmented and modeled. Other organs were created by transforming an existing adult male or female full-body computer model (developed from visible human data) to match the framework defined by the segmented organs, referencing the organ volume and anthropometry data in ICRP Publication 89. A Monte Carlo program previously developed and validated for dose simulation on the LightSpeed VCT scanner was used to estimate patient-specific organ dose, from which effective dose and risks of cancer incidence were derived. Patient-specific organ dose and effective dose were compared with patient-generic CT dose quantities in current clinical use: the volume-weighted CT dose index ($CTDI_{vol}$) and the effective dose derived from the dose-length product (DLP).

Results: The effective dose for the CT examination of the newborn patient (5.7 mSv) was higher but comparable to that for the CT examination of the teenager patient (4.9 mSv) due to the size-based clinical CT protocols at our institution, which employ lower scan techniques for smaller patients. However, the overall risk of cancer incidence attributable to the CT examination was much higher for the newborn (2.4 in 1000) than for the teenager (0.7 in 1000). For the two pediatric-aged patients in our study, $CTDI_{vol}$ underestimated dose to large organs in the scan coverage by 30%–48%. The effective dose derived from DLP using published conversion coefficients differed from

that calculated using patient-specific organ dose values by −57% to 13%, when the tissue weighting factors of ICRP 60 were used, and by −63% to 28%, when the tissue weighting factors of ICRP 103 were used.

Conclusions: It is possible to estimate patient-specific radiation dose and cancer risk from CT examinations by combining a validated Monte Carlo program with patient-specific anatomical models that are derived from the patients' clinical CT data and supplemented by transformed models of reference adults. With the construction of a large library of patient-specific computer models encompassing patients of all ages and weight percentiles, dose and risk can be estimated for any patient prior to or after a CT examination. Such information may aid in decisions for image utilization and can further guide the design and optimization of CT technologies and scan protocols. © *2011 American Association of Physicists in Medicine*. [DOI: 10.1118/1.3515864]

Key words: CT, computed tomography, Monte Carlo, radiation, dose, risk, patient-specific, NURBS

I. INTRODUCTION

Since its introduction in the 1970s, computed tomography (CT) has expanded its application areas from neurological and oncological examinations in the early stage to examinations of a wide range of disease conditions, including those in young patients. With the expanding use of CT comes great concern over its radiation exposure.[1] By its nature, CT delivers substantially higher radiation dose to patients than conventional radiography. Adding to the radiation burden are (a) repeated or redundant examinations, (b) technical factors not adapted to patient size, and (c) inconsistent use of technical factors from time to time in the same patient. To effectively manage CT radiation, it is highly desirable that the radiation dose and potential cancer risk associated with each CT scan of each patient be reported and documented. Such a patient-specific dose and risk reporting system could guide the design of CT protocols, ensure consistent use of technical parameters, and aid in decisions for image utilization, especially in situations where multiple examinations have been performed or are being considered.

The current dose-reporting method, however, is patient-generic; a patient's dosimetry report only includes quality assurance dose quantities such as CT dose index[2] (CTDI) measured in a standard-size cylindrical phantom (e.g., 32 cm diameter phantom for adult body). While a myriad of physical[3,4] and computerized[5–10] anthropomorphic phantoms exist for dosimetric applications, they only represent standard or limited patient sizes at discrete reference ages (e.g., 0, 1, 5, 10, and 15 years of age) and do not reflect the size and hence dose variation from patient to patient. Furthermore, the current protocol designs rely on dose as a surrogate for the risk of cancer incidence, neglecting the fact that the same dose delivered to two patients may entail substantially different risks due to age and gender differences. Figure 1 illustrates the strong dependence of risk on age and gender using lung cancer and all cancers combined as examples.

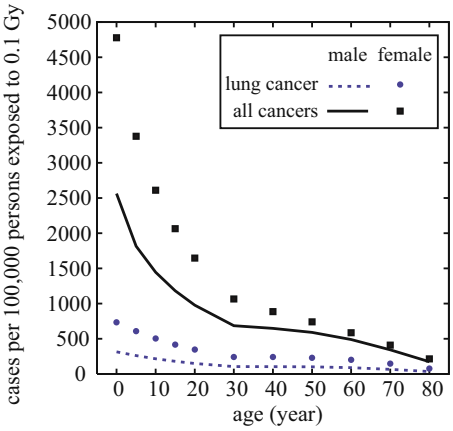

FIG. 1. Lifetime attributable risks of cancer incidence tabulated in BEIR VII report (Ref. 22). Risks for lung cancer and all cancers are shown to illustrate the strong dependence of risk on age and gender.

In Part I of this work (see Ref. 47), we reported the development of a Monte Carlo program for simulating dose from CT examinations and the validation of this program in cylindrical and anthropomorphic phantoms for both axial and helical scans. The goal of this paper was to apply this program to actual patients to develop a method for patient-specific dose and risk estimation.

II. MATERIALS AND METHODS

II.A. Patients

The study included two patients: A newborn (5 weeks, female) and a teenager (12 years, male). Both patients underwent 64-slice CT examinations (LightSpeed VCT, GE Healthcare, Waukesha, WI) of the chest, abdomen, and pelvis at our institution in 2006 using our size-based pediatric protocols at the time that employed fixed tube currents (Table I).

The study was approved by our institutional review board (IRB), who determined that it was in compliance with the Health Insurance Portability and Accountability Act (HIPAA), and did not require informed consent.

II.B. Patient-specific computer models

For each patient, a full-body computer model was created from the patient's clinical CT data. The initial anatomy of the model was defined by segmenting the patient's CT images using a software application developed in our laboratory. The heart, liver, gall bladder, stomach, spleen, and kidneys were

TABLE I. CT examinations undergone by the two patients in our study. Each patient underwent a combined chest-abdomen-pelvis (CAP) examination consisting of a chest scan and an abdomen-pelvis scan.

	Newborn (5 weeks, female)		Teenager (12 years, male)	
	Chest	Abdomen-pelvis	Chest	Abdomen-pelvis
Image coverage	From lung apex to top of liver	From 0.75 cm above top of liver to 1.25 cm below bottom of ischium	From 1 cm above lung apex to top of liver	From 1 cm above top of liver to just above bottom of ischium
kVp	100	120	120	120
mA	55	70	90	110
Gantry rotation period (s)	0.4	0.4	0.4	0.4
Scan FOV (bowtie filter)	Pediatric body (small)	Pediatric body (small)	Medium body (medium)	Medium body (medium)
Collimation (mm)	40	40	40	40
Pitch	0.984	0.984	1.375	1.375
Slice thickness (mm)	3.75	3.75	5	5
Reconstruction interval (mm)	2.5	2.5	5	5
Overranging distance (cm)	4.72	4.72	6.40	6.40

manually segmented by contouring from each CT slice. The lungs and bones were semiautomatically segmented using CT number thresholding. Once a data set was segmented, three-dimensional polygon models were generated for each structure using the marching cubes algorithm.[11,12] Three-dimensional NURBS surfaces were then fitted to the polygon models using NURBS modeling software (Rhinoceros, McNeel North America, Seattle, WA) to create the initial patient-specific model.

Other organs and structures, not easily segmented or visible in the scan coverage, were defined by morphing an existing male or female full-body adult model (developed from visible human data)[13] to match the framework defined by the segmented organs. The morphing was performed manually using the affine transformations of rhinoceros. The volumes of the organs and structures defined in this manner were checked and scaled, if necessary, to match age-interpolated organ volume and anthropometry data in ICRP Publication 89.[19] More details on the process of model creation is reported in another publication.[14]

The full-body models of the newborn female and the teenager male patients possessed a total of 44 and 43 organs, respectively, including most of the radiosensitive organs defined by ICRP Publication 103 (Ref. 15) (Table II). Figure 2 illustrates surface-rendered views of the three-dimensional anatomy in the computer models of the two patients.

While each patient's three-dimensional CT data set may also serve as his/her patient-specific computer model,[16] the full-body models in our study allowed dose to be estimated for not only organs within the image volume, but also organs in the overranging distance (additional scan length necessary for data interpolation in helical reconstruction)[17] and those outside the scan coverage.

II.C. Organ dose simulations

The NURBS model of each patient was "positioned" on a model of the CT table (see Part I of this work) in a supine position with arms elevated above the head to mimic actual patient posture during CT examinations. The models were voxelized at 0.5 and 1 mm isotropic resolutions for the newborn and the teenager, respectively. Each organ/structure was assigned a material (Table II) based on the elemental composition and mass density information tabulated in ICRU Publication 46 (Ref. 18) with the exception of the skeleton (a homogeneous mixture of its component tissues), for which the material information published by Cristy and Eckerman[5] for the skeletons of newborn and adult was used for the newborn and the teenager patients, respectively.

For each patient, organ dose simulation was performed for the chest scan and the abdomen-pelvis scan separately (Table I). The dose from the entire examination was then calculated as the sum of the dose from the two scans. The scan coverage in the actual patient examinations (Table I) was reproduced in the simulations. The total scan length in a helical scan was calculated as the image coverage plus the overranging distance (Table I). The overranging distance was estimated from the scanner console parameters as "table speed (cm/s) × total scan time (s)–image coverage (cm)." In a helical scan, the x-ray tube starting angle is not fixed and thus different each time (per private communication with the manufacturer). As the exact tube starting angles in the patients' examinations were unknown (part of CT raw data, not archived), each scan was simulated six times with the tube starting angle differing by 60° each time.

Energy deposited in organs and tissues was tallied and used to calculate dose. Because bone marrow and bone surface were not explicitly modeled, the following methods were used to estimate dose to these two organs. To assess dose to the red bone marrow, volume-averaged photon fluence spectrum was tallied individually at each skeletal site and used to calculated dose to the red bone marrow via the fluence-to-dose conversion coefficients published by Cristy and Eckerman.[5] A single active marrow dose was then calculated as its skeletal average using the age-dependent fractional distribution of active marrow tabulated in ICRP Publication 89.[19] Dose to the bone surface was approximated by the mass-weighted average of dose to the homogenous bones as recommended by Lee *et al.*[20]

TABLE II. Summary of organs in the computer models of the two patients.

Organ/structure	Density (g cm^{-3}) [h]	Material (ICRU 46)[h]	Mass (g)[j]	
			Newborn (5 weeks, female)	Teenager (12years, male)
Respiratory system				
Pharynx-larynx[a]	1.03	Average soft tissue[i]	1.6	17.3
Trachea-bronchi	1.03	Average soft tissue	1.0	13.7
Lungs	0.26	Lung (adult, healthy, inflated)	57.9	445.3
Alimentary system				
Esophagus	1.03	Average soft tissue	1.5	18.0
Stomach[b]	1.03	Average soft tissue	39.4	282.9
Pancreas	1.03	Average soft tissue	9.2	82.1
Liver	1.03	Average soft tissue	104.5	961.5
Gall bladder	1.03	Average soft tissue	4.1	24.6
Small intestine	1.03	Average soft tissue	70.7	558.3
Large intestine	1.03	Average soft tissue	63.9	436.5
Circulatory system				
Heart	1.03	Average soft tissue	51.2	459.8
Urogenital system				
Kidneys	1.03	Average soft tissue	21.5	189.3
Urinary bladder	1.03	Average soft tissue	5.4	63.8
Prostate[c]	1.03	Average soft tissue	–	3.1
Testes	1.03	Average soft tissue	–	3.9
Ovaries	1.03	Average soft tissue	0.5	–
Uterus	1.03	Average soft tissue	3.2	–
Vagina	1.03	Average soft tissue	0.4	–
Skeletal system[d]				
Cranium	1.4[h]	Average skeleton[h]	257.5	941.9
Mandible	1.4	Average skeleton	20.5	99.4
Clavicles	1.4	Average skeleton	1.2	42.9
Scapulea	1.4	Average skeleton	6.3	164.6
Sternum	1.4	Average skeleton	2.5	32.1
Ribs	1.4	Average skeleton	25.5	302.9
Cervical vertebrae	1.4	Average skeleton	7.1	74.4
Thoracic vertebrae	1.4	Average skeleton	23.5	233.7
Lumbar vertebrae	1.4	Average skeleton	16.6	186.7
Pelvis	1.4	Average skeleton	25.6	492.6
Sacrum	1.4	Average skeleton	10.9	152.7
Upper humeri	1.4	Average skeleton	5.1	175.9
Lower humeri	1.4	Average skeleton	3.7	125.1
Radii, ulnae	1.4	Average skeleton	6.1	185.9
Wrist and hand bones	1.4	Average skeleton	4.6	132.1
Upper femora	1.4	Average skeleton	10.9	439.6
Lower femora	1.4	Average skeleton	15.0	543.9
Tibiae, fibiae, patellae	1.4	Average skeleton	21.5	765.5
Ankle and foot bones	1.4	Average skeleton	12.1	420.1
Integumentary system				
Skin (torso only)[e]	1.03	Average soft tissue	49.3	452.4
Additional organs/tissues				
Brain	1.03	Average soft tissue	400.3	1488.4
Eyes	1.03	Average soft tissue	6.8	14.6
Thyroid	1.03	Average soft tissue	1.6	11.2
Breasts[f]	0.96	Breast (50/50)	0.7	2.2
Thymus	1.03	Average soft tissue	16.3	37.5
Spleen	1.03	Average soft tissue	8.1	215.1
Adrenal glands	1.03	Average soft tissue	6.5	10.6
Residual soft tissues[g]	1.03	Average soft tissue	2348.2	30 226.5

[a]Combined organ of pharynx and larynx, combined organ of trachea and bronchi, and esophagus were modeled as tubular organs with air-fill lumens. The wall thickness of these tubular organs was assumed to be 2 mm for the newborn and 3 mm for the teenager. It was independently verified that, over the range of 1–3 mm, the effect of wall thickness on organ dose was less than 1%. Dose to combined organ of pharynx and larynx was used as a surrogate for dose to salivary glands, oral mucosa, and extrathoracic (ET) region.

[b]Alimentary tract organs (stomach, small intestine, large intestine), heart, gall bladder, and urinary bladder were modeled as single homogenous organs without

delineation of walls and contents. For alimentary tract organs, dose to the entire organ (wall and content) was used to approximate the dose to the radiosensitive wall lining. This is a reasonable approximation since the wall and the content are located in parallel to each other.
[c]Prostate, testes, ovaries, uterus, and vagina are gender-specific organs and were included in the models of their respective genders only.
[d]The skeleton was modeled as a homogeneous mixture of its component tissues, namely, cortical bone, trabecular bone, yellow marrow, red marrow, and various connective tissues. The atomic composition and mass density data published by Cristy and Eckerman (Ref. 5) for the skeletons of newborn and adult were used for the newborn and the teenager patients, respectively.
[e]The torso of the NURBS model of each patient was covered with a skin layer to allow dose estimations for the skin. The skin thickness was assumed to be 1 and 2 mm for the newborn and the teenager patients, respectively, resulting in a 1–2 voxel definition of the skin in the Monte Carlo simulations. Whole body skin dose was calculated as torso skin dose multiplied by the ratio of torso skin area to whole body skin area, where skin areas were estimated from the NURBS model of each patient.
[f]The breasts of each patient were located based on the body surface contours of the patient in his/her CT images and relative to the locations of other organs. They were modeled as homogenous organs with elemental composition defined according to the 50/50-breast in ICRU Publication 46 (Ref. 18). Since glandular breast tissue only starts developing in puberty (Ref. 46), the breasts of the newborn patient were likely to have little glandular tissue; however, in the BEIR VII report (Ref. 22), the lifetime attributable risk of breast cancer is the highest at age of zero. Thus, even the breast tissue of a newborn has some radiosensitive structure, the dose to which was approximated by the dose to a 50/50-breast.
[g]Residual soft tissues included skeletal muscle, adipose tissue, cartilage, blood, lymphatic tissues, and connective tissues. Dose to residual soft tissues was used to approximate dose to skeletal muscle and lymphatic nodes.
[h]The atomic composition and mass density data tabulated in ICRU Publication 46 (Ref. 18) were used for all organs and tissues with the exception of the skeleton (see footnote d).
[i]Average soft tissue of adult male was used.
[j]Organ/tissue mass in the voxel models.

In terms of simulation time, using a single processor on a 2.3 GHz Linux server with 20 GB of random access memory (RAM), 80 million photon histories (6 h runtime plus another 30 min of input/output operation time) were used to simulate each CT scan of each patient, resulting in relative dose error of less than 1% for all organs in the scan coverage and less than 3% for other organs.

II.D. Effective dose and cancer risk calculations

Simulated organ dose values were used to calculate effective dose for each CT scan of each patient as

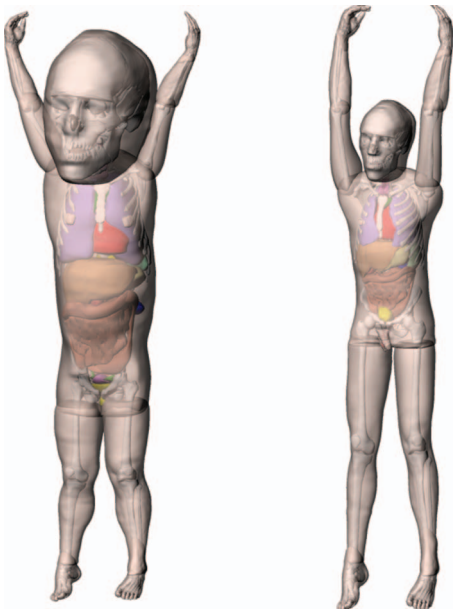

FIG. 2. Surface rendered views of the three-dimensional anatomy in the computer models of the newborn female (5 weeks old, left) and the teenager male (12 years old, right) patients in this study.

$$E = \sum_T w_T H_T, \tag{1}$$

where H_T is the equivalent dose for organ/tissue T and w_T is the tissue weighting factor defined by ICRP Publication 103.[15] Dose to radiosensitive organs that were not explicitly modeled was approximated by dose to neighboring organs (Table II). Dose to the testes or the ovaries was used as dose to the gonads. The w_T for the reminder tissues was applied to the arithmetic mean dose of the 13 remainder tissues of each gender. Breast dose was included in the calculation of effective dose for both patients.

While widely used as a surrogate for radiation risk, effective dose does not reflect individual patient risk; the tissue weighting factors are mean values representing averages over both gender and age.[15] Therefore, to more accurately estimate individual patient risks, we further implemented a metric of risk, termed "risk index," and defined as

$$\text{risk index} = \sum_T r_T(\text{gender, age}) H_T, \tag{2}$$

where r_T is the gender-, age-, and tissue-specific risk coefficient (cases/100 000 exposed to 0.1 Gy) for lifetime attributable risk of cancer incidence. The metric of risk index (RI) presented here was adopted from the recently proposed concept of effective risk.[21] We chose to use the term risk *index*, as opposed to effective risk, to reflect the inherent uncertainties associated with estimating risks for individual patients, who might have different radiosensitivities due to genetic predispositions or hormonal profiles.

Values of r_T are available for leukemia and for cancers of eight to nine high-risk organs of each gender at discrete ages of 0, 5, 10, 15, 20, 30, 40, 50, 60, 70, and 80 years,[22] from which we linearly interpolated the values of r_T at other ages. Cancers of other radiosensitive organs share a collective risk coefficient (r_{other}).[22] The collective risk to these other organs was calculated as[23]

$$R_{\text{other}} = \sum_{T\in\{\text{other organs}\}} r_T H_T = \sum_{T\in\{\text{other organs}\}} \left(\frac{w_T}{\Sigma_{T\in\{\text{other organs}\}} w_T} r_{\text{other}} \right) H_T = r_{\text{other}} \left(\frac{\Sigma_{T\in\{\text{other organs}\}} w_T H_T}{\Sigma_{T\in\{\text{other organs}\}} w_T} \right), \quad (3)$$

where the other radiosensitive organs included heart, kidney, gall bladder, spleen, pancreas, adrenal glands, thymus, small intestine, salivary glands, extrathoracic region, lymph node, muscle, oral mucosa, bone surface, brain, skin, testes (male only), and esophagus. Among these organs, the reminder tissues, as defined by ICRP Publication 103,[15] were each assigned a tissue-weighting factor of 0.01. As the individual r_T values for these "other organs" are unavailable, in Eq. (3), we assumed that the contribution of each r_T to the collective r_{other} is proportional to the sex- and age-averaged radiosensitivity of organ T relative to all the other organs, as represented by ratio of the tissue weighting factors.

To compare patient-specific dose estimation with the current dose-reporting method, dose to large organs inside the scan coverage were compared with volume-averaged CTDI (CTDI_{vol}).[24] Furthermore, effective dose calculated using the organ dose of specific patients was compared with the effective dose derived from the dose-length product (DLP).[24] For each patient's each CT scan, CTDI_{vol} was calculated from the technical reference manual of the LightSpeed VCT scanner using the tables of CTDI_{100} and technique adjustment factors. The scan FOV used for each patient (Table I) determined the corresponding CTDI phantom size: 16 cm diameter and 32 cm diameter phantoms for the newborn and the teenager patients, respectively. When calculating DLP, the total scan length included the overranging distance. The CTDI_{vol} and DLP values calculated in this way agreed with those from patients' dosimetry reports to within about 5%. To convert from DLP to effective dose, we used the conversion coefficients (often referred to as the k factors) published by Shrimpton *et al.*,[25,26] which are the most frequently used conversion coefficients in the literature[27,28] and are included in the AAPM Report No. 26.[24] The conversion coefficients for 0-year-old patients (chest scan: $k=0.039$; abdomen-pelvis scan: $k=0.049$) and 10-year-old patients (chest scan: $k=0.013$; abdomen-pelvis scan: $k=0.015$) were used for the newborn and the teenager patients in this study, respectively. Considering that these conversion coefficients were developed based on the older ICRP Publication 60,[29] effective dose was also calculated using the tissue weighting factors of ICRP Publication 60. This allowed the difference between patient-specific and patient-generic dose estimations to be demonstrated without the confounding effect of the change in tissue weighting factors.

Lastly, we assessed the need for creating a full-body computer model for dose and risk estimations, i.e., the need for modeling organs and structures outside of the image coverage. For simplicity, the effective dose and risk index were recalculated with dose and risk to organs completely outside of the image coverage set to zero. While doing so was not identical to performing dose simulations with partial-body computer models based entirely on the patients' clinical CT data, it provided a rough assessment of the need for modeling organs and structures outside of the image coverage.

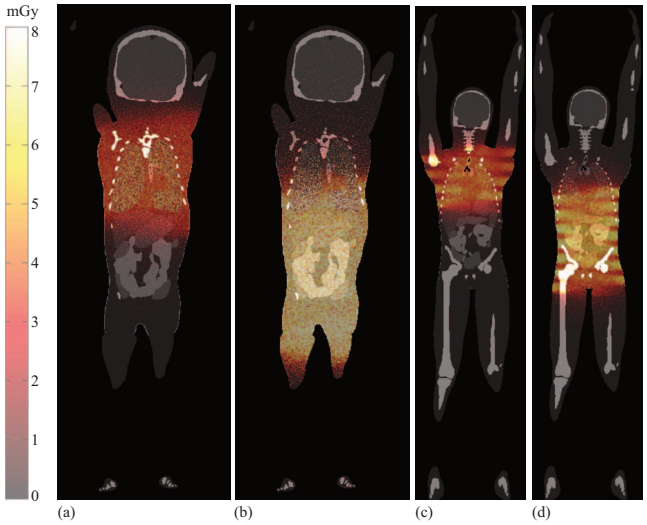

FIG. 3. Coronal dose distributions in the two patients, resultant from their CT examinations: (a) chest scan of the newborn patient, (b) abdomen-pelvis scan of the newborn patient, (c) chest scan of the teenager patient, and (d) abdomen-pelvis scan of the teenager patient. The tube starting angle was 0° (12 o'clock) for all scans. The coronal plane was taken about half-way in between the anterior and posterior surfaces of each patient. The computer model of each patient with organs shown on a gray scale was overlaid with a semitransparent colored image of the dose distribution. The noise in the dose distribution is reflective of the limited number of photos used in the simulations. As organ dose was an average over the entire organ volume, the uncertainty associated with organ dose was less than 1% for all organs in the scan coverage and less than 3% for other organs (see Sec. II C).

III. RESULTS

Examples of dose distributions in the two patients from their CT examinations are illustrated in Fig. 3. The dose distribution was more uniform in the newborn patient (pitch of 0.984) than in the teenager patient (pitch of 1.375). As a result of the overranging distance, a large portion of the abdomen (chest) was irradiated in the chest (abdomen-pelvis) scan.

Table III summarizes the organ and effective dose values. The corresponding risks of cancer incidence are tabulated in Table IV. For the newborn patient, lung dose from the abdomen-pelvis scan was comparable to that from the chest scan (Table III). For both patients, the effective dose from the abdomen-pelvis scan was close to double that from the chest scan. For the entire chest-abdomen-pelvis examination (consisting of a chest scan and an abdomen-pelvis scan), the organ and effective dose of the newborn patient was one to two times that of the teenager patient (Table III, last column). However, the newborn patient had about ten times greater risk of thyroid cancer than the teenager patient (Table IV, last column). The risk index (overall cancer risk) of the newborn patient was about four times that of the teenager patient (Table IV, last column).

TABLE III. Organ and effective dose of the two patients from their CT examinations. Each patient underwent a combined chest-abdomen-pelvis (CAP) examination consisting of a chest scan and an abdomen-pelvis scan. Each dose value is the average over six tube starting angles. The percentage value in the bracket is the coefficient of variation (standard deviation × 100%/average) across tube starting angles.

	Dose (mGy)										
	Newborn (5 weeks, female)					Teenager (12 years, male)					Dose ratio[b]
	Chest		Abdomen-pelvis		CAP[a]	Chest		Abdomen-pelvis		CAP[a]	CAP
Respiratory system											
Pharynx-larynx	1.86	(5%)[c]	0.23	(1%)[c,d]	2.09	1.03	(17%)[c]	0.06	(3%)[c,d]	1.09	1.9
Trachea-bronchi	3.28	(0%)	0.58	(2%)[c,d]	3.86	3.88	(3%)	0.38	(2%)[c,d]	4.26	0.9
Lungs	3.68	(0%)	3.54	(3%)	7.22	3.93	(0%)	2.54	(2%)	6.47	1.1
Alimentary system											
Esophagus	3.20	(0%)	1.55	(3%)[c]	4.75	3.35	(2%)	1.37	(1%)	4.72	1.0
Stomach	1.36	(7%)[c]	6.36	(0%)	7.72	1.53	(17%)[c]	5.04	(1%)	6.57	1.2
Pancreas	0.34	(2%)[c,d]	6.38	(1%)	6.72	0.55	(4%)[c,d]	4.91	(1%)	5.46	1.2
Liver	2.02	(8%)[c]	6.56	(0%)	8.58	1.57	(13%)[c]	4.93	(0%)	6.50	1.3
Gall bladder	1.02	(16%)[c]	6.88	(1%)	7.90	0.37	(9%)[c,d]	5.52	(8%)	5.89	1.3
Small intestine	0.27	(4%)[c]	7.07	(0%)	7.34	0.15	(4%)[c,d]	5.57	(1%)	5.72	1.3
Large intestine	0.24	(7%)[c]	6.76	(0%)	7.00	0.10	(3%)[c,d]	5.08	(1%)	5.18	1.4
Circulatory system											
Heart	3.56	(0%)	4.16	(7%)	7.72	4.14	(1%)	2.61	(10%)	6.75	1.1
Urogenital system											
Kidneys	1.52	(8%)[c]	6.08	(0%)	7.60	0.75	(11%)[c]	4.52	(0%)	5.27	1.4
Urinary bladder	0.04	(3%)[c,d]	6.30	(2%)	6.34	0.02	(2%)[c,d]	5.20	(3%)	5.22	1.2
Prostate		-		-	-	0.01	(5%)[c,d]	4.05	(2%)	4.06	-
Testes		-		-	-	0.00	(14%)[c,d]	5.10	(15%)	5.10	-
Ovaries	0.05	(5%)[c,d]	6.28	(2%)	6.33		-		-	-	-
Uterus	0.04	(2%)[c,d]	6.18	(2%)	6.22		-		-	-	-
Vagina	0.03	(5%)[c,d]	6.24	(2%)	6.27		-		-	-	-
Skeletal system											
Bone surface	1.81	(2%)	3.36	(0%)	5.17	1.45	(1%)	2.68	(0%)	4.13	1.3
Red bone marrow	0.83	(1%)	1.57	(0%)	2.40	1.01	(1%)	1.91	(0%)	2.92	0.8
Integumentary system											
Skin	0.54	(1%)	1.70	(1%)	2.24	0.60	(1%)	1.24	(0%)	1.84	1.2
Additional organs/tissues											
Brain	0.12	(1%)[c,d]	0.05	(1%)[c,d]	0.17	0.07	(2%)[c,d]	0.01	(3%)[c,d]	0.08	2.1
Eyes	0.08	(7%)[c,d]	0.03	(2%)[c,d]	0.11	0.05	(3%)[c,d]	0.01	(8%)[c,d]	0.06	1.8
Thyroid	2.85	(1%)	0.36	(3%)[c,d]	3.21	4.47	(10%)	0.23	(2%)[c,d]	4.70	0.7
Breasts	2.88	(1%)	1.62	(31%)[c]	4.50	3.64	(23%)	1.04	(42%)[c]	4.68	1.0
Thymus	3.53	(0%)	0.73	(3%)[c]	4.26	4.05	(4%)	0.51	(4%)[c,d]	4.56	0.9
Spleen	2.63	(3%)	5.79	(1%)	8.42	1.60	(18%)	4.60	(1%)	6.20	1.4
Adrenal glands	2.04	(2%)	6.05	(0%)	8.09	1.29	(4%)[c]	4.07	(2%)	5.36	1.5
Residual soft tissues	0.99	(1%)	2.81	(1%)	3.80	0.73	(0%)	1.44	(0%)	2.17	1.8
Effective dose (mSv)	1.64	(1%)	4.04	(2%)	5.68	1.78	(5%)	3.15	(1%)	4.93	1.2

[a]Dose from the combined chest-abdomen-pelvis (CAP) examination, i.e., the summation of dose from the chest scan and that from the abdomen-pelvis scan.
[b]Dose ratio equals dose to the newborn patient from her CAP examination over dose to the teenager patient from his CAP examination.
[c]Organs completely outside of the image coverage (Table I).
[d]Organs completely outside of the scan coverage (scan coverage equals image coverage plus overranging distance, see Table I).

For most organs, the dose uncertainty due to the random tube starting angle was less than 10% (Table III). The uncertainty was generally higher at pitch of 1.375 compared to pitch of 0.984. The uncertainty was higher for small peripheral organs (e.g., breast, testes) and for organs on the edge of the scan coverage (e.g., gall bladder in the chest scan of the newborn patient; pharynx-larynx, stomach, liver, kidney, spleen in the chest scan of the teenager patient; breasts in the abdomen-pelvis scans of both patients). Tube starting angle had a small effect on effective dose and risk index (<5%).

For the two pediatric-aged patients in this study, $CTDI_{vol}$ underestimated dose to large organs in the scan coverage by 30%–48% (Table V). The effective dose derived from DLP differed from that estimated using patient-specific organ dose values by −57% to 13%, when the tissue weighting factors of ICRP 60 were used and by −63% to 28%, when the tissue weighting factors of ICRP 103 were used (Table V). Compared with ICRP 103 based effective dose, ICRP 60 based effective dose was 15%–16% lower for chest scans, but 14%–16% higher for abdomen-pelvis scans.

TABLE IV. Lifetime risks of cancer incidence for the two patients attributable to their CT examinations. Each patient underwent a combined CAP examination consisting of a chest scan and an abdomen-pelvis scan. Each risk value is the average over six tube starting angles. The percentage value in the bracket is the coefficient of variation (standard deviation × 100%/average) across tube starting angles.

	Lifetime attributable risk of cancer incidence (cases/1000 exposed)										Risk ratio[b]
	Newborn (5 weeks, female)					Teenager (12 years, male)					
	Chest		Abdomen-pelvis		CAP[a]	Chest		Abdomen-pelvis		CAP[a]	CAP
Thyroid Bancer	0.179	(1%)	0.023	(3%) [c,d]	0.202	0.020	(10%)	0.001	(2%) [c,d]	0.021	9.6
breast cancer	0.335	(1%)	0.189	(31%) [c,d]	0.524	-	-	-	-	-	-
Lung cancer	0.269	(0%)	0.259	(3%)	0.528	0.080	(0%)	0.052	(2%)	0.132	4.0
Stomach cancer	0.014	(7%) [c]	0.064	(0%)	0.078	0.008	(17%)[c]	0.026	(1%)	0.034	2.3
Liver cancer	0.006	(8%) [c]	0.018	(0%)	0.024	0.006	(13%)[c]	0.020	(0%)	0.026	0.9
Colon cancer	0.005	(7%) [c,d]	0.148	(0%)	0.153	0.002	(3%)[c,d]	0.117	(1%)	0.119	1.3
Bladder cancer	0.001	(3%) [c,d]	0.133	(2%)	0.134	0.000	(2%) [c,d]	0.074	(3%)	0.074	1.8
Prostate cancer	-	-	-	-	-	0.000	(5%) [c,d]	0.026	(2%)	0.026	-
Ovary cancer	0.001	(5%) [c,d]	0.065	(2%)	0.066	-	-	-	-	-	-
Uterus cancer	0.000	(2%) [c,d]	0.031	(2%)	0.031	-	-	-	-	-	-
Leukemia	0.015	(1%)	0.029	(0%)	0.044	0.012	(1%)	0.022	(0%)	0.034	1.3
Other cancer	0.250	(1%)	0.403	(1%)	0.653	0.055	(2%)	0.143	(8%)	0.198	3.3
Risk index	1.075	(0%)	1.361	(5%)	2.436	0.184	(1%)	0.481	(2%)	0.665	3.7

[a]Risk from the combined chest-abdomen-pelvis (CAP) examination, i.e., the summation of risk from the chest scan and that from the abdomen-pelvis scan.
[b]Risk ratio equals risk to the newborn patient from her CAP examination over risk to the teenager patient from his CAP examination.
[c]Cancer risks to organs that were completely outside of the image coverage.
[d]Cancer risks to organs that were completely outside of the scan coverage.

Excluding the dose to organs completely outside of the image coverage resulted in an underestimation of effective dose by 4%–22% (Table VI). The underestimation was smaller for abdomen-pelvis scans. Excluding the risks to organs completely outside of the image coverage resulted in an underestimation of risk index by 0%–19% (Table VI). The underestimation was the largest for the abdomen-pelvis scan of the female (newborn) patient due to the exclusion of breast cancer risk.

IV. DISCUSSION

In this study, we demonstrated that it is possible to estimate patient-specific radiation dose and cancer risk from CT examinations by combining a validated Monte Carlo program with patient-specific anatomical models that are derived from the patients' clinical CT data and supplemented by transformed models of reference adults. While patient-specific dose estimations have been pursued in the past, they were either limited to providing dose for only the imaged part of the body[16,30] or limited to patients whose cadavers had undergone a whole-body scan.[31] Although the dose and risk estimates reported in our study were strictly patient-specific only for the segmented organs inside the image volume, as these organs receive the highest dose, the resultant effective dose and risk index estimates were indicative of the specific patients in their entirety.

For the newborn patient, lung dose from the abdomen-pelvis scan was comparable to those from the chest scan (Table III) due to both the overranging distance and the higher technique (higher kVp and mA) used in the abdomen-pelvis scan. For both patients, the effective dose from the abdomen-pelvis scan was close to double that from the chest scan. This can be attributable to the higher technique (kVp and/or mA) and the larger irradiated body volume in the abdomen-pelvis scan.

It is generally accepted that when the same scan technique is used, a smaller patient receives higher radiation dose.[31,32] Due to the size-based pediatric CT protocols in use at our institution, which use lower scan techniques for smaller patients, organ and effective dose received by the newborn patient was comparable to that of the teenager patient (Table III, last column). However, when the risks of cancer incidence were assessed, the newborn patient had about ten times greater risk of thyroid cancer than the teenager patient (Table IV, last column) due to age and gender differences. The risk index (overall cancer risk) of the newborn patient was about four times that of the teenager patient (Table IV, last column). As the same dose may entail substantially different risks to patients of different ages and genders, patient-specific risk estimates should be used together with dose estimates to guide the design and optimization of CT technologies and scan protocols. Knowledge of the risks to a specific patient may potentially influence the decisions for image utilization, especially in situations where multiple examinations are being performed or considered. Furthermore, patient-specific risk information may be extremely helpful for institutional review of scientific investigations using CT examinations. Finally, patient-specific dose and risk estimations afford more individualized and expanded application of dose tracking from medical radiation exposures.[33,34]

Our study showed that the dose distribution was more uniform in the newborn patient (pitch of 0.984) than in the teenager patient (pitch of 1.375). As a result, the dose uncertainty due to the random tube starting angle was generally

TABLE V. Comparison between volume-weighted CT dose index ($CTDI_{vol}$) and patient-specific organ dose, and comparison between effective dose derived from DLP using published conversion coefficients and effective dose estimated using patient-specific organ dose values.

	Newborn (5 weeks, female)		Teenager (12 years, male)	
	Chest	Abdomen-pelvis	Chest	Abdomen-pelvis
Large organ dose (mGy) [a]				
Approximated by $CTDI_{vol}$ [b]	2.21	4.77	2.24	2.74
Estimated for specific patient	3.62	6.82	4.04	5.25
Discrepancy	−39%	−30%	−44%	−48%
Effective dose (mSv)				
Derived from DLP[c]	1.18	5.18	0.66	1.57
Estimated for specific patient (ICRP 103)	1.64	4.04	1.78	3.15
Estimated for specific patient (ICRP 60)	1.37	4.60	1.52	3.64
Discrepancy (DLP VS ICRP 103)	−28%	28%	−63%	−50%
Discrepancy (DLP VS ICRP 60)	−14%	13%	−56%	−57%
Discrepancy (ICRP 60 VS ICRP 103)	−16%	14%	−15%	16%

[a]Average dose to large organs inside the scan coverage, represented by lung and heart for the chest scan and liver and small intestine for the abdomen-pelvis scan.
[b]The scan FOV used for each patient (Table I) determined the corresponding CTDI phantom size: 16 cm diameter and 32 cm diameter phantoms for the newborn and the teenager patients, respectively.
[c]The DLP was 30.34 and 105.77 mGy- cm for chest and abdomen-pelvis scans of the newborn patient, and 51.14 and 104.99 mGy- cm for chest and abdomen-pelvis scans of the teenager patient.

larger at pitch of 1.375 (Table III). However, one should not interpret this result as "the lower the helical pitch, the more uniform the dose distribution, and hence the smaller the effect of tube starting angle." At a pitch less than unity, the hot spots created by beam overlap can also lead to nonuniform dose distribution along the z-axis.[35] The effect of tube starting angle was reduced by the presence of scattered radiation. As peripheral/surface organs received lower scattered radiation compared to central organs, the dose uncertainty was higher for peripheral organs, especially small peripheral organs (e.g., breasts and testes). The effect of tube starting angle was also found to be large for organs on the edge of the scan coverage (e.g., gall bladder in the chest scan of the newborn patient; pharynx-larynx, stomach, liver, kidney, spleen in the chest scan of the teenager patient, breasts in the abdomen-pelvis scans of both patients). This can be explained both by the uncertainty in the fraction of organ volume covered by the primary radiation and the low scattered radiation from neighboring organs outside of the scan coverage.

To further demonstrate the inadequacy of the current patient-generic dose reporting method, we compared $CTDI_{vol}$ with patient-specific dose to large organs in the scan coverage. For the two patients in our study, $CTDI_{vol}$ grossly underestimated (−30% to −48%) dose to large organs in the scan coverage, primarily because the newborn and the teenager patients had average trunk diameters of 9.7 and 21.7 cm, respectively, much smaller than the diameters of the standard CTDI phantoms (i.e., 16 and 32 cm diameter PMMA or equivalently 18 and 36 cm diameter water[36]), on which the respective $CTDI_{vol}$ values were based. As such, $CTDI_{vol}$ should not be used as a surrogate for patient dose in CT.

Furthermore, we showed that the effective dose derived

TABLE VI. Comparison between effective dose and risk index calculated using dose to all radiosensitive organs and those calculated using only dose to imaged radiosensitive organs.

	Newborn (5 weeks, female)		Teenager (12 years, male)	
	Chest	Abdomen-pelvis	Chest	Abdomen-pelvis
Effective dose (mGy)				
Include all radiosensitive organs	1.64	4.04	1.78	3.15
Include only imaged radiosensitive organs[a]	1.28	3.75	1.47	3.01
Discrepancy	−22%	−7%	−17%	−4%
Risk index (cases/1000 exposed)				
Include all radiosensitive organs	1.075	1.361	0.184	0.481
Include only imaged radiosensitive organs[a]	0.990	1.099	0.157	0.479
Discrepancy	−8%	−19%	−15%	0%

[a]Exclude dose and risk to organs that were completely outside of the image coverage as annotated in Tables III and IV

from DLP can differ substantially from that calculated using patient-specific organ dose values, even when the tissue weighting factors of ICRP 60 were used. The DLP-to-effective dose conversion coefficients (k factors) of Shrimpton *et al.*[25,26] were developed based on ICRP 60 and a family of mathematical/stylized reference phantoms developed by Cristy and Eckerman.[5] The 0-year-old and the 10-year-old reference phantoms in this family had equivalent trunk diameters of 11.2 and 21.6 cm, respectively, comparable to the body size of the newborn and the teenager patients in this study, who had average trunk diameters of 9.7 and 21.7 cm, respectively. The discrepancies in effective dose found for the newborn patient (chest scan: −14%; abdomen-pelvis scan: 13%) were most likely due to the differences in anatomy between the newborn patient and 0-year-old reference phantom. The latter had a trunk defined by an elliptical cylinder with organs defined by simple geometric shapes. The particular large discrepancies in effective dose found for the teenager patient (chest scan: −56%; abdomen-pelvis scan: −57%) can be attributed to yet another factor: the mismatch in CTDI phantom. The teenager patient in our study was scanned using the medium body scan field-of-view, which corresponded to a 32 cm diameter CTDI phantom, whereas all the k factors for pediatric patients were developed assuming CTDI values in a 16 cm diameter phantom. Thus, the k factors for pediatric patients can significantly underestimate effective dose, if the pediatric patient is not scanned using a scan field-of-view type that corresponds to a 16 cm diameter CTDI phantom.

We found that effective dose based on organ dose and the tissue weighting factors of ICRP 60 differ relative to ICRP 103 values by −15% to −16% for chest scans and by 14%–16% for abdomen-pelvis scans. Similar discrepancies have also been reported by other authors[28] and are attributable to the increase in breast weighting factor from 0.05 to 0.12 and decrease in gonad weighting factor from 0.20 to 0.08.

Our study also quantified the changes in effective dose (4%–22%) and risk index (0%–19%) when dose and risk to organs outside of the image coverage are assumed to be zero (Table VI). It may be argued that, for the abdomen-pelvis scan of the teenager patient, the changes in effective dose (4%) and risk index (0%) are in consequential. However, as many patients undergo sequential CT examinations over an extended period of time, small underestimations can accumulate and result in significant dose and risk errors. The results highlight the importance of developing full-body patient models for dose and risk estimations.

It is important to note that in this study we did not use the concept of effective dose as originally defined. Effective dose was defined by ICRP for a *reference hermaphrodite adult*; the tissue weighting factors are gender- and age-averaged values, and the organ dose should be gender-averaged values as well.[15] Thus, in principle, effective dose is not suitable for individual patients. However, the concept has been widely applied to patients of various sizes, ages, and genders[27,31,37] and to individual patients.[31] Recently, the limitations of effective dose have been discussed in the literature, and there have been intensive debates over whether the concept is applicable to medical exposure and whether it should be replaced.[21,38–41] Our calculation of effective dose using patient-specific organ dose values, while not being exactly as defined by ICRP, served two purposes: (a) it provided patient dose estimates using a concept that the medical imaging community is currently familiar with and thus can put in context with other dose studies and (b) it approximates the effective dose to a patient population (including both genders) who has similar anatomy and body habitus as the patient whose organ dose values were used in the effective dose calculation.

The patient-specific method developed in this study can be applied to report and document CT radiation in the following three foreseeable manners.

(a) With the development of a library of representative patient-specific computer models, the method reported in this study can be employed to create a database of dose and risk estimates for patients of all ages and weight percentiles. The database can then be used to estimate patient-specific dose and risk for any new patient by matching the patient to an existing patient in the library based on age, gender, and body habitus.

(b) An alternative to the first approach, the database of dose and risk estimates can be used to draw correlations between dose/risk, patient size/age/gender, and technical factors, i.e.,

$$\text{dose} = f(\text{technical factors, patient size}), \tag{4}$$

$$\text{risk} = g(\text{technical factors, patient size, age, gender}). \tag{5}$$

In a preliminary study of pediatric chest CT examinations,[42] we showed that dose to large organs in the scan coverage is strongly correlated with the mid-chest equivalent diameter of a patient (r=−0.93 to −0.99). Such correlations likely exist for a wider range of patient sizes and for other body sections. Furthermore, other investigators have demonstrated, with small numbers of patients and scanner models, that when organ dose simulated by Monte Carlo methods are normalized by CTDI values, the variations across CT scanner models are small.[43,44] Thus, our method may be used to provide *normalized* dose and risk in the format of Eqs. (4) and (5) that are independent of scanner models.

(c) If the process of creating a full-body computer model from each patient's clinical CT data can be fully automated, it would be possible to estimate patient-specific dose and risk in real time immediately following a patient's CT examinations. In this study, we used 80 million photon histories (6.5 h user time) to simulate each CT scan of each patient to obtain relative dose errors of less than 1% for any organ inside the scan coverage and less than 3% for any organ outside of the scan coverage. In fact, ~7 million photon histories (1 h

user time) were sufficient to achieve relative dose errors of less than 1% for all organs in the scan coverage and less than 10% for other organs. With the implementation of GPU technology,[45] the speed of Monte Carlo simulations may soon meet the requirements for real-time applications. Considering the uncertainties associated with Monte Carlo simulations (point dose discrepancies of −17% to 13% between simulation and measurement for helical scans, see Ref. 47), it is possible that the dose difference among patients of similar body habitus is smaller than or comparable to the uncertainties associated with the Monte Carlo simulation. If future studies show that is the case, there will be no need to create a patient-specific model for every patient, and the first two approaches can be used.

Our study has several limitations. First, both patients in our study underwent fixed-tube-current examinations (tube current modulation was not the standard practice in 2006). If the same patients were examined at our institution today, tube-current-modulation techniques would have been used with the maximum tube currents similar to the mA values in Table I. Thus, the dose and risk to the two patients would have been lower than that reported in Tables III and IV. Second, the accuracy of our risk estimations is limited by the accuracy/uncertainties of the current cancer risk models,[22] which are largely based on the life-span studies of atomic-bomb survivors and limited number of studies on occupational exposures. Furthermore, as the risk coefficients are still statistical averages over many individuals of the same gender and similar age, they cannot reflect individual vulnerability due to genetic factors. As such, the cancer risks we reported do not represent the true risk of an individual from his/her CT examination but rather our current best knowledge of the potential risk to a patient from his/her CT examination, knowing the patient's age and gender. Therefore, care should be exercised when interpreting the risk results. Nevertheless, the patient-specific risk information, as presented by our study, represents a step forward beyond effective dose toward personalized patient care.

V. CONCLUSION

It is possible to estimate patient-specific radiation dose and cancer risk from CT examinations by combining a validated Monte Carlo program with patient-specific anatomical models that are derived from the patients' clinical CT data and supplemented by transformed models of reference adults. With the construction of a large library of patient-specific computer models encompassing patients of all ages and weight percentiles, dose and risk can be estimated for any patient prior to or after a CT examination. Patient-specific estimates can be included in a patient's dosimetry and medical record to track radiation exposure history from medical imaging, serving as a basis from which to better assess the cost-benefit ratio when making decisions about CT examinations in the clinical setting. They can further guide the design and optimization of CT technologies and scan protocols.

ACKNOWLEDGMENTS

The work was supported in part by grants from GE Healthcare and the National Institutes of Health (Grant No. RO1 EB001838).

[a]Electronic mail: samei@duke.edu

[1]D. J. Brenner and E. J. Hall, "Computed tomography–an increasing source of radiation exposure," N. Engl. J. Med. **357**, 2277–2284 (2007).
[2]T. B. Shope, R. M. Gagne, and G. C. Johnson, "A method for describing the doses delivered by transmission x-ray computed tomography," Med. Phys. **8**, 488–495 (1981).
[3]C. L. Chapple, S. Willis, and J. Frame, "Effective dose in paediatric computed tomography," Phys. Med. Biol. **47**, 107–115 (2002).
[4]L. M. Hurwitz, T. T. Yoshizumi, P. C. Goodman, R. C. Nelson, G. Toncheva, G. B. Nguyen, C. Lowry, and C. Anderson-Evans, "Radiation dose savings for adult pulmonary embolus 64-MDCT using bismuth breast shields, lower peak kilovoltage, and automatic tube current modulation," AJR, Am. J. Roentgenol. **192**, 244–253 (2009).
[5]M. Cristy and K. F. Eckerman, "Specific absorbed fractions of energy at various ages from internal photon sources," Oak Ridge National Laboratory Report No. ORNL/TM-8381.
[6]N. Petoussi-Henss, M. Zanki, U. Fill, and D. Regulla, "The GSF family of voxel phantoms," Phys. Med. Biol. **47**, 89–106 (2002).
[7]C. Lee, J. L. Williams, and W. E. Bolch, "Whole-body voxel phantoms of paediatric patients–UF Series B," Phys. Med. Biol. **51**, 4649–4661 (2006).
[8]C. Lee, D. Lodwick, J. Hurtado, D. Pafundi, J. L. Williams, and W. E. Bolch, "The UF family of reference hybrid phantoms for computational radiation dosimetry," Phys. Med. Biol. **55**, 339–363 (2010).
[9]V. F. Cassola, V. J. Lima, R. Kramer, and H. J. Khoury, "FASH and MASH: Female and male adult human phantoms based on polygon mesh surfaces: I. Development of the anatomy," Phys. Med. Biol. **55**, 133–162 (2010).
[10]A. Christ, W. Kainz, E. G. Hahn, K. Honegger, M. Zefferer, E. Neufeld, W. Rascher, R. Janka, W. Bautz, J. Chen, B. Kiefer, P. Schmitt, H. P. Hollenbach, J. Shen, M. Oberle, D. Szczerba, A. Kam, J. W. Guag, and N. Kuster, "The Virtual Family–development of surface-based anatomical models of two adults and two children for dosimetric simulations," Phys. Med. Biol. **55**, N23–N38 (2010).
[11]W. E. Lorensen and H. E. Cline, "Marching cubes: A high resolution 3D surface construction algorithm," Proceedings of the 14th Annual Conference on Computer Graphics and Interactive Techniques, 1987, pp. 163–169.
[12]W. Schroeder, K. W. Martin, and B. Lorensen, *The Visualization Toolkit: An Object-Oriented Approach to 3D Graphics*, 3rd ed. (Kitware, New York, 2006).
[13]W. P. Segars, B. M. W. Tsui, E. C. Frey, and E. K. Fishman, "Extension of the 4D NCAT phantom to dynamic x-ray CT simulation," IEEE Nuclear Science Symposium Conference Record, 2004, Vol. 5, pp. 3195–3199.
[14]G. M. Sturgeon, X. Li, S. Mendonca, D. P. Frush, E. Samei, and W. P. Segars, "Series of anatomically detailed NURBS-based phantoms for pediatric CT research," Med. Phys. (to be published).
[15]ICRP, "The 2007 recommendations of the international commission on radiological protection," ICRP Publication No. 103.
[16]P. Deak, M. van Straten, P. C. Shrimpton, M. Zankl, and W. A. Kalender, "Validation of a Monte Carlo tool for patient-specific dose simulations in multi-slice computed tomography," Eur. Radiol. **18**, 759–772 (2008).
[17]A. J. van der Molen and J. Geleijns, "Overranging in multisection CT: Quantification and relative contribution to dose–comparison of four 16-section CT scanners," Radiology **242**, 208–216 (2006).
[18]ICRU, "Photon, electron, proton and neutron interaction data for body tissues," ICRU Report No. 46, 1992.
[19]ICRP, "Basic anatomical and physiological data for use in radiological protection: Reference values," ICRP Publication No. 89, 2002.
[20]C. Lee, A. P. Shah, and W. E. Bolch, "An assessment of bone marrow and

bone endosteum dosimetry methods for photon sources," Phys. Med. Biol. **51**, 5391–5407 (2006).
[21]D. J. Brenner, "Effective dose: A flawed concept that could and should be replaced," Br. J. Radiol. **81**, 521–523 (2008).
[22]NRC, *Health Risks from Exposure to Low Levels of Ionizing Radiation—BEIR VII* (The National Academies Press, Washington, DC, 2006).
[23]D. Brenner, C. Elliston, E. Hall, and W. Berdon, "Estimated risks of radiation-induced fatal cancer from pediatric CT," AJR, Am. J. Roentgenol. **176**, 289–296 (2001).
[24]"The measurement, reporting, and management of radiation dose in CT," AAPM Report No. 96, 2008.
[25]P. Shrimpton, *Assessment of Patient dose in CT. NRPB-PE/1/2004* (NRPB, Chilton, 2004).
[26]P. C. Shrimpton, M. C. Hillier, M. A. Lewis, and M. Dunn, "National survey of doses from CT in the UK: 2003," Br. J. Radiol. **79**, 968–980 (2006).
[27]K. E. Thomas and B. Wang, "Age-specific effective doses for pediatric MSCT examinations at a large children's hospital using DLP conversion coefficients: A simple estimation method," Pediatr. Radiol. **38**, 645–656 (2008).
[28]J. A. Christner, J. M. Kofler, and C. H. McCollough, "Estimating effective dose for CT using dose-length product compared with using organ doses: Consequences of adopting International Commission on Radiological Protection publication 103 or dual-energy scanning," AJR, Am. J. Roentgenol. **194**, 881–889 (2010).
[29]ICRP, "The 1990 recommendations of the international commission on radiological protection," ICRP Publication No. 60.
[30]G. Jarry, J. J. DeMarco, U. Beifuss, C. H. Cagnon, and M. F. McNitt-Gray, "A Monte Carlo-based method to estimate radiation dose from spiral CT: From phantom testing to patient-specific models," Phys. Med. Biol. **48**, 2645–2663 (2003).
[31]J. J. DeMarco, C. H. Cagnon, D. D. Cody, D. M. Stevens, C. H. McCollough, M. Zankl, E. Angel, and M. F. McNitt-Gray, "Estimating radiation doses from multidetector CT using Monte Carlo simulations: Effects of different size voxelized patient models on magnitudes of organ and effective dose," Phys. Med. Biol. **52**, 2583–2597 (2007).
[32]E. L. Nickoloff, A. K. Dutta, and Z. F. Lu, "Influence of phantom diameter, kVp and scan mode upon computed tomography dose index," Med. Phys. **30**, 395–402 (2003).
[33]E. S. Amis, Jr., P. F. Butler, K. E. Applegate, S. B. Birnbaum, L. F. Brateman, J. M. Hevezi, F. A. Mettler, R. L. Morin, M. J. Pentecost, G. G. Smith, K. J. Strauss, and R. K. Zeman, "American College of Radiology white paper on radiation dose in medicine," J. Am. Coll. Radiol. **4**, 272–284 (2007).
[34]http://rpop.iaea.org/RPOP/RPoP/Content/News/smart-card-project.htm.
[35]D. Zhang, M. Zankl, J. J. DeMarco, C. H. Cagnon, E. Angel, A. C. Turner, and M. F. McNitt-Gray, "Reducing radiation dose to selected organs by selecting the tube start angle in MDCT helical scans: A Monte Carlo based study," Med. Phys. **36**, 5654–5664 (2009).
[36]J. M. Boone, E. M. Geraghty, J. A. Seibert, and S. L. Wootton-Gorges, "Dose reduction in pediatric CT: A rational approach," Radiology **228**, 352–360 (2003).
[37]C. Lee, C. Lee, R. J. Staton, D. E. Hintenlang, M. M. Arreola, J. L. Williams, and W. E. Bolch, "Organ and effective doses in pediatric patients undergoing helical multislice computed tomography examination," Med. Phys. **34**, 1858–1873 (2007).
[38]D. Brenner and W. Huda, "Effective dose: A useful concept in diagnostic radiology?" Radiat. Prot. Dosim. **128**, 503–508 (2007).
[39]C. J. Martin, "Effective dose: How should it be applied to medical exposures?" Br. J. Radiol. **80**, 639–647 (2007).
[40]C. J. Martin, "The application of effective dose to medical exposures," Radiat. Prot. Dosim. **128**, 1–4 (2007).
[41]C. Borrás, W. Huda, and C. G. Orton, "Point/counterpoint. The use of effective dose for medical procedures is inappropriate," Med. Phys. **37**, 3497–3500 (2010).
[42]X. Li, E. Samei, W. P. Segars, G. M. Sturgeon, J. G. Colsher, and D. P. Frush, "Patient-specific dose estimation for pediatric chest CT," Med. Phys. **35**, 5821–5828 (2008).
[43]P. C. Shrimpton, D. Hart, M. C. Hiller, B. F. Wall, and K. Faulkner, "Survey of CT practice in the UK. 1. Aspects of examination frequency and quality assurance," NRPB Report No. 248, 1991.
[44]A. C. Turner, M. Zankl, J. J. DeMarco, C. H. Cagnon, D. Zhang, E. Angel, D. D. Cody, D. M. Stevens, C. H. McCollough, and M. F. McNitt-Gray, "The feasibility of a scanner-independent technique to estimate organ dose from MDCT scans: Using CTDIvol to account for differences between scanners," Med. Phys. **37**, 1816–1825 (2010).
[45]X. Jia, X. Gu, J. Sempau, D. Choi, A. Majumdar, and S. B. Jiang, "Development of a GPU-based Monte Carlo dose calculation code for coupled electron-photon transport," Phys. Med. Biol. **55**, 3077–3086 (2010).
[46]D. U. Silverthorn, *Human Physiology: An Integrated Approach*, 3rd ed. (Pearson/Benjamin Cummings, San Francisco, 2004).
[47]X. Li, E. Samei, W. P. Segars, G. M. Sturgeon, J. G. Colsher, G. Toncheva, T. T. Yoshizumi, and D. P. Frush, "Patient-specific radiation dose and cancer risk estimation in CT: Part I. Development and validation of a Monte Carlo program," Med. Phys. **37**, 397–407 (2010).